Effect of cold spray parameters on surface roughness, thickness and adhesion of copper based composite coating on aluminium alloy 6061 T6 substrate

Ling Shao [1, 2, 3], Na Xue [1, 3], Weiwei Li [1, 3], Song Liu [4], Zhibiao Tu [1, 3], Yingwei Chen [2], Jitang Zhang [1, 3], Sheng Dai [1, 3], Qijie Liu [2], Xinxing Shi [1], Tianle Wang [1], Mengliang Chen [5], Yingqi Huang [2], FeilongXu [1], Liu Zhu [1, 3, *]

[1] *Zhejiang Provincial Key Laboratory for Cutting Tools, Taizhou University, Taizhou 318000, P. R. China*

[2] *Taizhou Key Laboratory of Medical Devices and Advanced Materials, Research Institute of Zhejiang University-Taizhou, Taizhou 318000, P. R. China*

[3] *Taizhou Clean Carbon Technology Company Limited, Taizhou 318020, P. R. China*

[4] *Zhejiang Shuoshi Machinery Company Limited, Shaoxing 312073, P. R. China*

[5] *School of Materials Science and Engineering, Zhejiang Sci-Tech University, Hangzhou 310000, P. R. China*

Abstract Solid state cold spray technique was employed for depositing the copper-coated graphite reinforced copper based composite coatings on aluminium alloy 6061 T6 substrate under different process parameters. The optimum process parameters of the cold sprayed coatings were predicted in terms of surface roughness, thickness and adhesion. The surface roughness was measured using a 3D profilometer, the thickness and element constitution were detected by an optical microscope and scanning electron microscope furnished with an energy dispersive spectral analyzer, and the adhesion was detected by scratch test method. The results show that when the coating is not oxidized, the copper-coated graphite reinforced copper based composite coating at 800 °C, 5.5 MPa possesses the lowest surface roughness, the maximum thickness and the highest adhesion among the cold sprayed coatings. In addition, the surface roughness, thickness and adhesion of the deposited coatings are all linear with particle velocity.

Keywords: Copper based composite coating; Cold spray; Surface roughness; Thickness; Adhesion

1. Introduction

Owing to light weight, high toughness, excellent processing performance, good electrical conductivity and thermal conductivity, and relatively low cost, aluminum alloys are widely used in various industrial applications, such as military and civil buildings, automobile and aircraft manufacturing industries [1, 2]. However, aluminum alloys suffer disadvantages in terms of low hardness, poor wear resistance and easy deformation [3]. It is necessary that suitable surface modification treatment technique is adopted to promote electrical conductivity, wear resistance and surface hardness of aluminium alloy. Copper-coated graphite reinforced copper based composites (Cu@Gr/CBC) overcome the problem of no wetting between copper (Cu) and graphite, and combine attractive properties of Cu and graphite, exhibiting high electrical conductivity, good

*Corresponding author: Professor Liu Zhu. Zhejiang Provincial Key Laboratory for Cutting Tools, Taizhou University, Taizhou 318000, P. R. China. Email address: zhuliu@tzc.edu.cn.

thermal conductivity, and low friction coefficient [4, 5]. Therefore, Cu@Gr/CBC coatings are suitable as coatings deposited on aluminum alloys to promote electrical and mechanical properties of aluminum alloys.

Various coating technologies are implemented to prepare coating on aluminum alloys, such as thermal spraying [6, 7], chemical vapor deposition (CVD) [8, 9], laser surfacing [10, 11], physical vapor deposition (PVD) [12, 13], plasma electrolytic oxidation (PEO) [14, 15], anodizing [16, 17], and ion implantation [18]. As an emerging coating technique, solid state cold spray (CS) technology avails kinetic energy to deposit various coatings on different substrates, instead of combining kinetic and thermal energies like the high velocity oxyfuel (HVOF) spray technology [19]. Due to the sprayed material not melt, it is allowed to obtain very dense coatings without oxidation or diffusion into the substrate [20].

There are diverse vital issues which determine the quality of deposited coatings, such as surface roughness, thickness, adhesion and so on. It is crucial to find these optimal preparation conditions for producing high-quality coating on substrate. The adhesion between coating and substrate is a complex phenomenon, and depends on the preparation parameters. To control the numerous parameters of CS (related to spray parameters and feedstock powder), adhesion between coating and substrate can be promoted [21]. Based on the above-mentioned point, it is necessary to apply an appropriate method to assess coating adhesion. There are some methods to examine the adhesive property of the coatings, such as tensile test [22], hang test with a kettle bell [23], scratch test [24], indentation test [25], peel test [26] and blister test [27]. An examination approach of the adhesion of coatings relies on the sort of coating and the substrate. Among the diverse approaches, scratch test is one of the quickest and most effective methods to determine the coating adhesion [28]. Scratch test with a coneshaped or Berkovich indenter is a widely applied technology to detect the adhesion between coating and substrate [29-31]. The scratch test technique was adopted to test the single lane and single layer coatings in this work.

For producing high-quality Cu@Gr/CBC coatings on aluminum alloy 6061 T6 (AA6061 T6) substrate, it is necessary to study the single lane and single layer coatings first. In this study, single lane and single layer coatings were deposited to AA6061 T6 substrate at various spraying parameters by CS technology. The appearance, surface roughness, thickness, element constitution and adhesion of the coatings were examined with the corresponding testing techniques.

2. Experimental details

AA6061 T6 (Jiangsu Annan Metal Product Co., Ltd., Xinghua, China) plate of size 100 × 100 × 3 mm was used as the substrate material, having the chemical composition presented in Table 1. Before the deposition process, all substrate surfaces were ground with a SJK 9070F dry sand blasting machine, followed by ultrasonic cleaning with alcohol. A gas atomized Cu powder (99.99%, Nangong City Chunxu Metal Material Factory, Xingtai, China) with a volume weighted mean particle size of 17.4 μm was used, and electroplated Cu-coated graphite (Cu@graphite) powder (30 wt.% graphite, Nangong City Jinnuo Welding Material Co., Ltd., Xingtai, China) with a volume weighted average particle size of 18.6 μm was used as the reinforcement. Cu and Cu@graphite powder mixtures of 7 wt.% Cu@graphite powder were homogenized in a QM-QX-4L MITR ball mill for 1 h with PTFE container and agate balls. Scanning electron microscopy (SEM, Hitachi S-4800) image of the morphology and microstructure of the mixture powders is shown in Fig. 1a, revealing that the Cu particles presented a near-spherical surface structure while the Cu@graphite particles had a core–shell structure. The mixture powders were detected using an X-

ray diffractometer (XRD, Bruker D8 Advance) with Cu K_α radiation in the 2θ range of 10°–90° at 3° per minute scanning speed and 0.02° scanning step (Fig. 1b). The particle size distribution of the mixture powders represented by a laser diffraction sizer (Mastersizer3000, Malvern Instruments Ltd., UK) is presented in Fig. 1c. The dimensions of the mixture powders are D_{10} = 9.11 µm, D_{50} = 20.9 µm, and D_{90} = 44.0 µm. $D_{10,\ 50,\ 90}$ indicate the maximal particle size diameter which includes 10, 50, 90% of the specimens (volume-weighted basis).

Table 1 Chemical composition (wt.%) of AA6061 T6 plate

Elements	Si	Cr	Cu	Fe	Mn	Ti	Zn	Mg	Al
6061 aluminum alloy plate	0.4-0.8	0.04-0.35	0.15-0.4	≤0.7	≤0.15	≤0.15	≤0.25	0.8-1.2	Balance

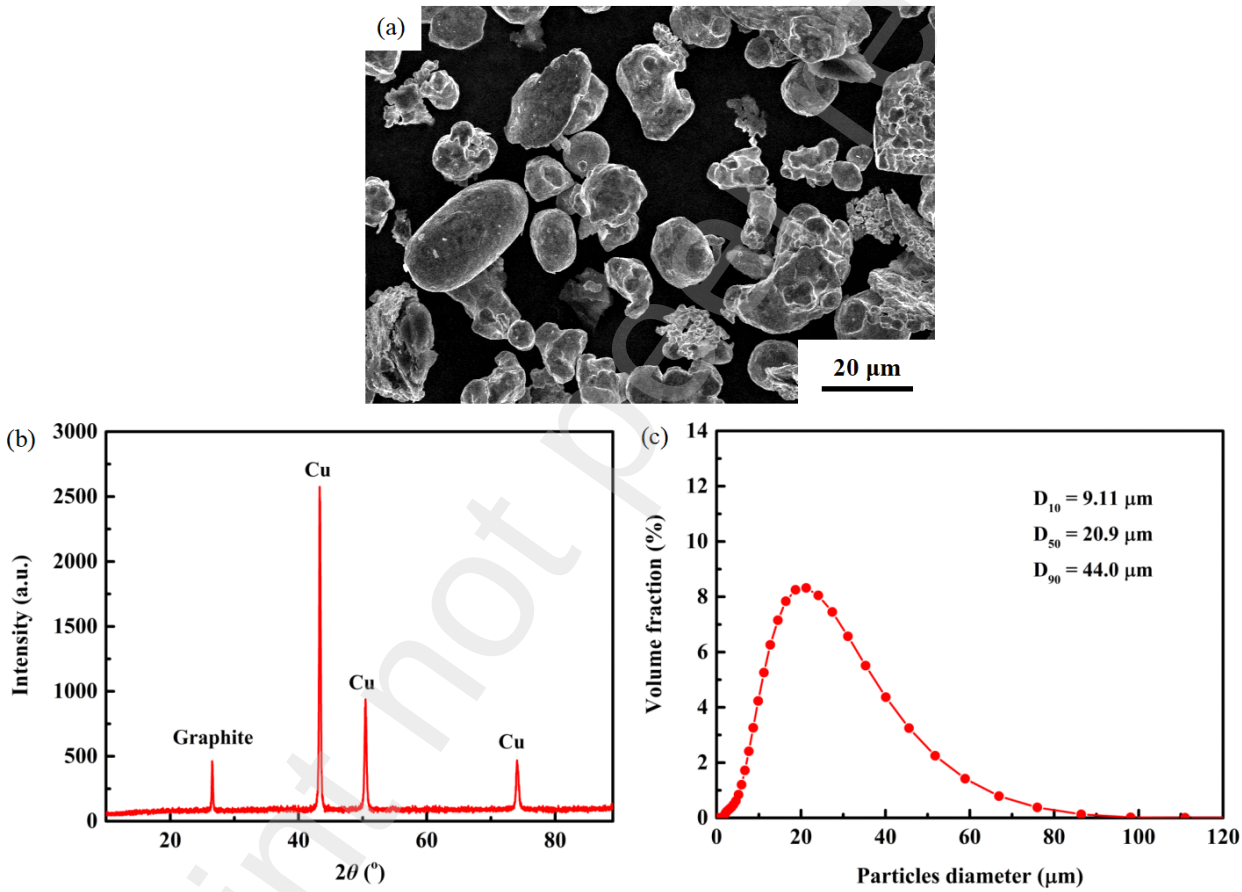

Fig. 1. SEM image showing the morphology of Cu and 7 wt.% Cu coated graphite mixture particles (a), XRD pattern presenting the phases of the mixture powders (b) and the size distribution curve of the mixture particles (c).

The single lane and single layer Cu@Gr/CBC coatings were prepared by cold spray PCS-100 system (Plasma Giken Co., Ltd., Osato, Saitama, Japan) furnished with a PNFC-010 convergent-divergent (de-Laval type) nozzle, and N_2 was applied as an accelerating gas, as shown in Fig. 2a. The spray gun was shifted at a line rate of 50 mm s^{-1} over the substrate at a constant stand-off distance of 20 mm. The gas flow of feeding was fixed at 180 SLM for all powder blends. The gas temperature was increased from 600 °C to 900 °C, and the gas pressure was changed from 4 MPa to 5.5 MPa at each gas temperature. The specific cold spray parameters are given in Table 2.

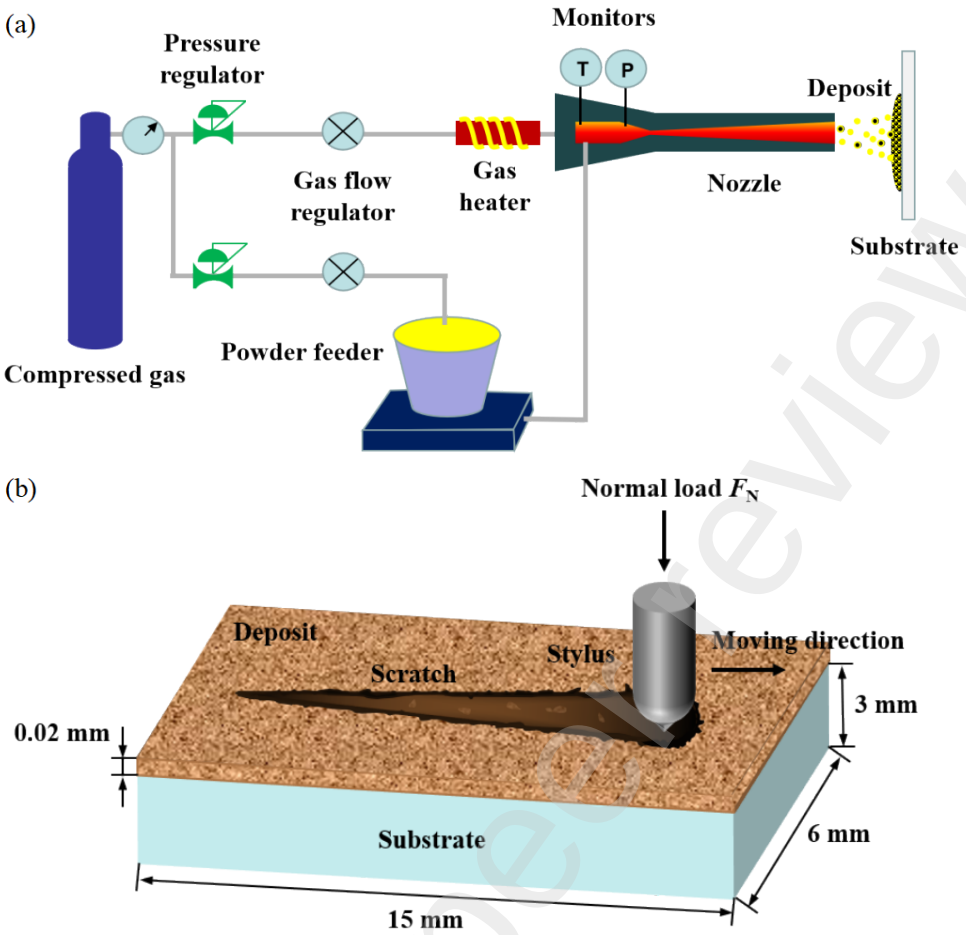

Fig. 2. Schematic diagrams of cold spray process (a) and scratch coating adhesion test (b).

Table 2 Deposition parameters of Cu@Gr/CBC coatings prepared by CS technology

Coating	gas temperature (°C)	Gas pressure (MPa)	Gas flow of feeding (SLM)	Traverse velocity (mm s^{-1})	Distance from the substrate (mm)	Deposition layer (layer)
1	900	5.5	180	50	20	1
2	900	5	180	50	20	1
3	900	4.5	180	50	20	1
4	900	4	180	50	20	1
5	800	5.5	180	50	20	1
6	800	5	180	50	20	1
7	800	4.5	180	50	20	1
8	800	4	180	50	20	1
9	700	5.5	180	50	20	1
10	700	5	180	50	20	1
11	700	4.5	180	50	20	1
12	700	4	180	50	20	1
13	600	5.5	180	50	20	1
14	600	5	180	50	20	1
15	600	4.5	180	50	20	1

16	600	4	180	50	20	1

Different technologies were employed to analyze surface roughness, thickness, microstructure and composition of the single lane and single layer Cu@Gr/CBC coatings. The surface roughness *R*a of the cold sprayed coatings was assessed via a Bruker Contour X100 3D profilometer (Bruker Biosciences Corporation, USA) for a resolution of 0.1 nm and maximum measuring range of 500 μm, installed with Bruker Vision software. Each reported *R*a value is an average of ten readings. To examine the thickness and study the microstructure of the coatings, the specimens were cut along the cross sections by wire cutting into a dimension of 10 mm × 10 mm × 3 mm. The cross sections of the specimens were ground with wet abrasive papers, mechanically polished to obtain mirror-polished sections, and ultrasonically cleaned in alcohol. The thickness was measured at the highest position of the coatings with an Zeiss Axio scope A1 optical microscope (OM, Carl Zeiss, Jena, Thuringia, Germany). The microstructure and element constitution were examined using OM and SEM equipped with an energy dispersive spectral analyzer (EDS).

The adhesion of the Cu@Gr/CBC coatings on AA6061 T6 substrate was determined using a WS-2005 scratch tester under 100 N total load, 100 N min^{-1} scratch velocity and 4 mm scratch length. The WS-2005 scratch tester was furnished with a three-sided pyramidal diamond (Berkovich) indenter of 0.2 mm tip radius for scratch testing. Figure 2b shows the schematic diagram of scratch coating adhesion test. Prior to testing, the thickness of the deposited coatings was controlled at 20 μm by grinding and measuring, and the surface of the coatings was polished to mirror. Scratch test was replicated three times for each specimen and the average value was taken as the coating adhesion. The scratch morphology was examined using SEM, and the coating adhesion was determined according to the coating shed position and the scratch length.

3. Results and discussion

3.1. Characterization

The typical appearance of the single lane and single layer Cu@Gr/CBC coating on AA6061 T6 substrate at 800 °C and 5.5 MPa is shown in Fig. 3a. A coating strip of 100 mm length and 6 mm width was sprayed on AA6061 T6 substrate. The microstructure of the cross section of the deposited coating is presented in Fig. 3b. As shown in Fig. 3b, the single lane and single layer coating is a sector shape deposited on substrate. Figure 3c is the magnified cross sectional micrograph of the coating in Fig. 3b. The coating is dense and only has a few porosities. Area scanning analysis was performed for the deposited coating at 800 °C and 5.5 MPa in Fig. 3d and the result shows that Cu was not oxidized during spraying process. However, the cold sprayed Cu@Gr/CBC coating was oxidized at 900 °C and 5.5 MPa by EDS analysis (Fig. 3f). Fig. 3d and 3f are the EDS analysis results of the area noted by rectangular box in Fig. 3c and 3e, respectively.

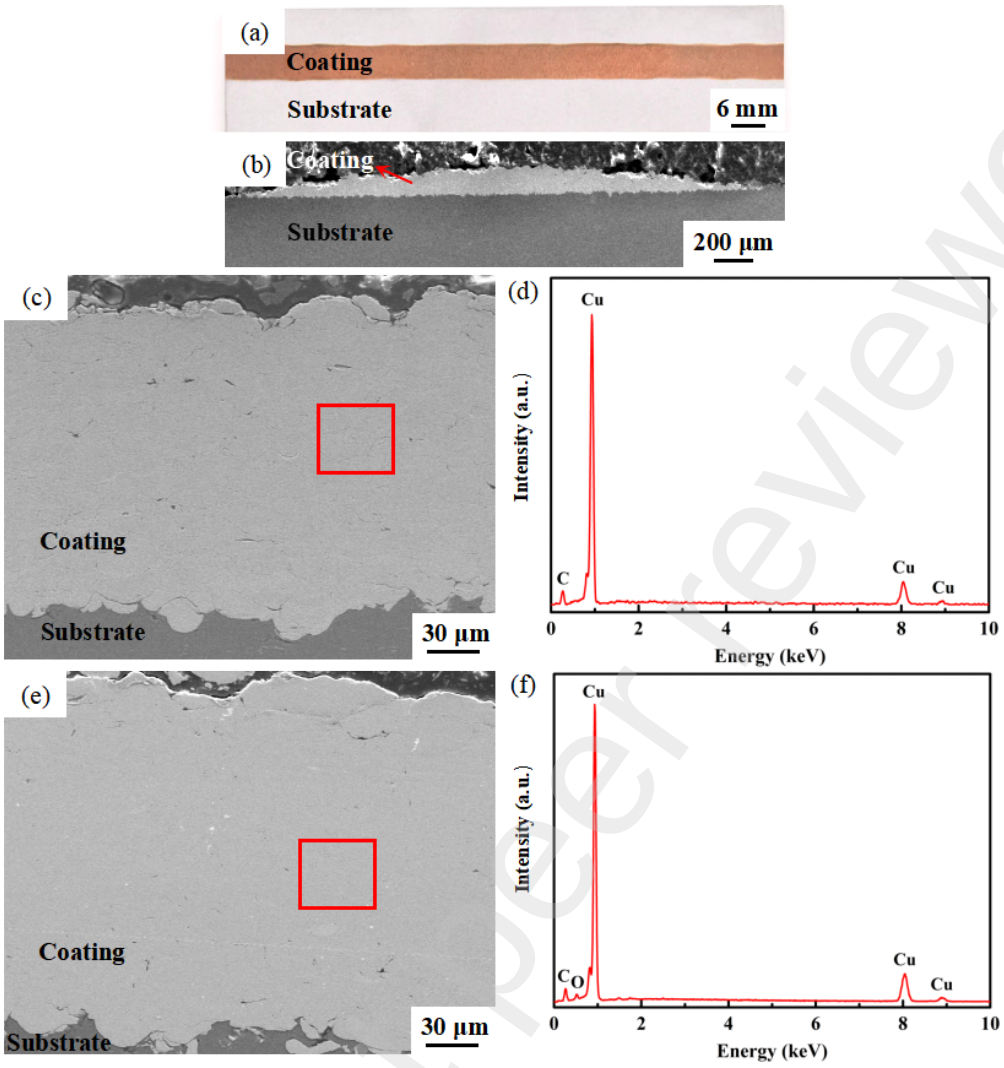

Fig. 3. Typical appearance of the single lane and single layer Cu@Gr/CBC coating on AA6061 T6 substrate at 800 °C and 5.5 MPa (a), SEM morphology of the cross section of the deposited coating (b), higher magnification photo of the deposited coating (c), EDS analysis result of the area noted by rectangular box in (c) (d), SEM micrograph of the cold sprayed coating at 900 °C and 5.5 MPa (e) and EDS analysis result of the area noted by rectangular box in (e) (f). The lightest area is coating and the gray area is substrate in (b), (c) and (e).

The surface morphology of the single lane and single layer Cu@Gr/CBC coating at 800 °C and 5.5 MPa is uneven and undulating (Fig. 3a). The *R*a of the Cu@Gr/CBC coatings obtained at various spraying parameters (Table 2) is shown in Fig. 4a. The *R*a of the coatings was between 7.05 and 12.69 µm, and sluggishly decreased with increasing gas pressure and gas temperature. By 3D surface morphology color mapping, the *R*a was apparently projected showing affluent color changes with the interweave of deep color and light color. Figures 4b-4e are the 3D surface morphology of coatings deposited at 800 °C and different gas pressures. The surface of the deposited coatings gets more and more flat with few depressions and bulges, whereas the colors of the surfaces of the cold sprayed coatings were more or less alike in the 3D surface morphology color mappings.

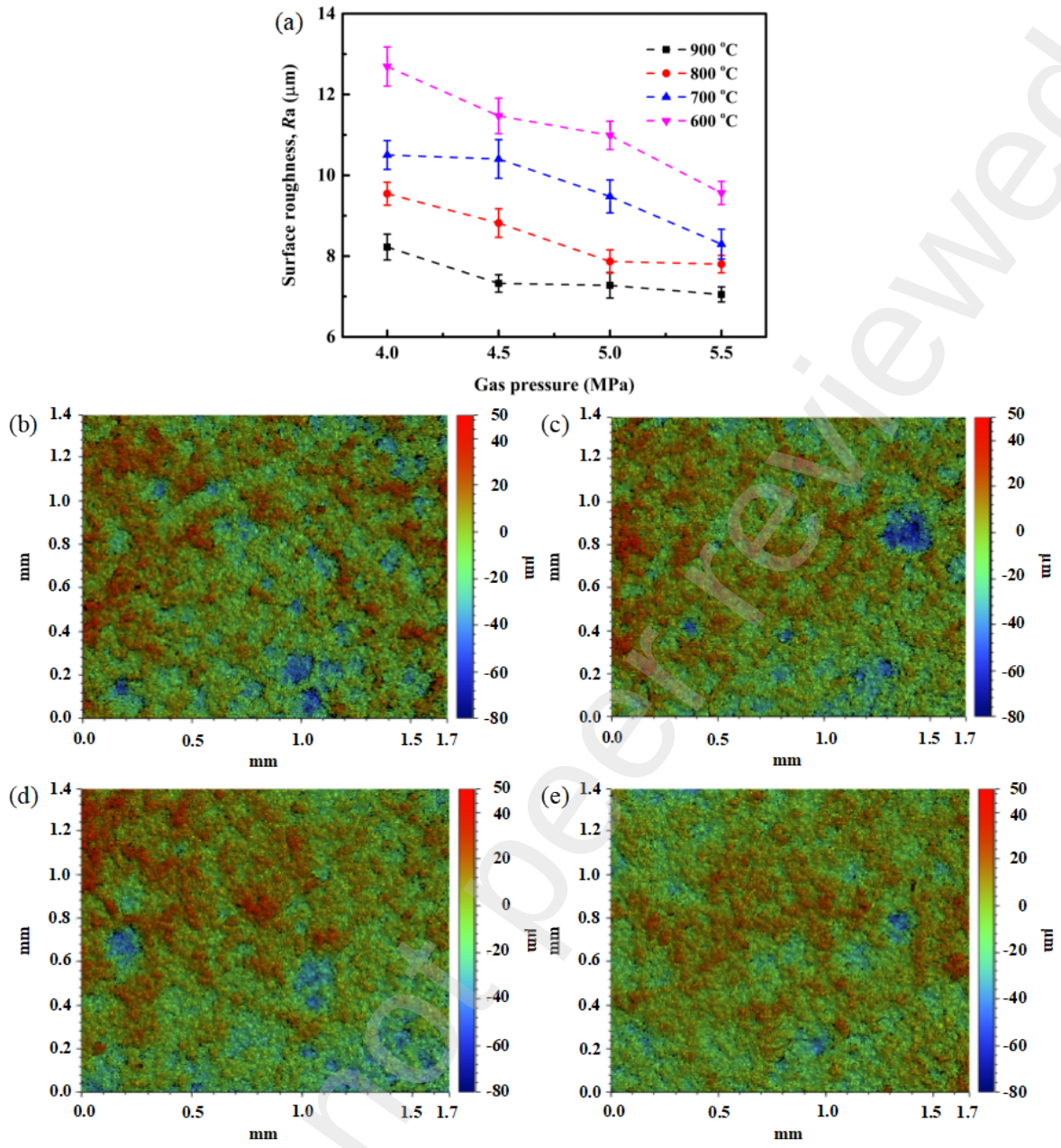

Fig. 4. Effect of cold spraying parameters on the surface roughness *R*a of the deposited Cu@Gr/CBC coatings on AA6061 T6 substrate (a), 3D surface morphology of coatings deposited at 800 °C and different gas pressures: 4 MPa (b), 4.5 MPa (c), 5 MPa (d) and 5.5 MPa (e).

The thickness of the single lane and single layer Cu@Gr/CBC coatings deposited on AA6061 T6 substrate with varying cold spray parameters is presented in Fig. 5. The thickness of the deposited coating increases significantly with increasing gas pressure and gas temperature. This is due to the higher the cold spray parameters (gas pressure and gas temperature) chosen, the more the powder materials in the stagnation zone are decelerated [32]. The highest thickness is 175.6 μm for the deposited coating at 900 °C and 5.5 MPa, and the lowest thickness is 72.8 μm for the deposited coating at 600 °C and 4 MPa. Figures 5b-5e are OM images for the thickness of coatings deposited at 800 °C and different gas pressures. It can been obviously seen that the coating thickness increases with increasing gas pressure. The porosities of the deposited coatings showed little difference.

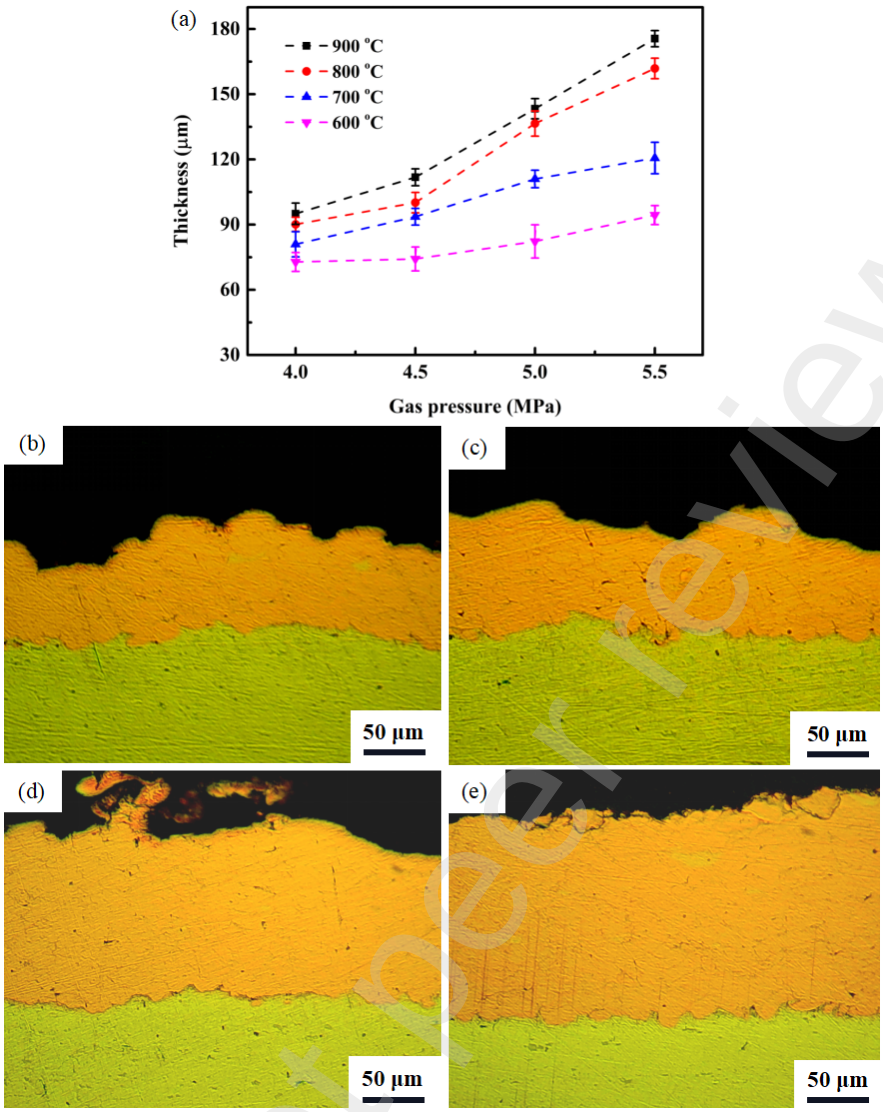

Fig. 5. Thickness of cold sprayed Cu@Gr/CBC coatings on AA6061 T6 substrate with varying deposited parameters (a), OM images showing the thickness of coatings deposited at 800 °C and different gas pressures: 4 MPa (b), 4.5 MPa (c), 5 MPa (d) and 5.5 MPa (e).

3.2. Adhesion

The adhesive property of the deposited coatings was examined using the scratch test method. Corresponding to the entire length of the scratch (L_{total}) about 4 mm, the total load is 100 N. The critical length of the scratch L_c (from the beginning point of the scratch to the delaminated position of the deposited coating), is defined as critical load that causes a failure event. The value of critical load is taken as an adhesion of the deposited coating with the substrate. The adhesion of the coatings was calculated as L_c divided by L_{total} and multiplied by a hundred. The formula [33] is:

$$\text{Adhesion} = \frac{L_c}{L_{total}} \times 100 \quad (1)$$

The unit of the coating adhesion is N. In general, adhesive failure indicates the delamination of coating from its substrate. Therefore, the critical load describes the adhesion of the deposited coating to the substrate.

In literatures [34, 35], it is mentioned that high peening influence of the powder materials and low processing temperature in the CS process result in high adhesion of the deposited coating.

However, the study results of the adhesion of Cu@Gr/CBC coatings on AA6061 T6 substrate are some differences. Figure 6a shows the adhesion of the Cu@Gr/CBC coatings on AA6061 T6 substrate under different spraying parameters. From Fig. 6a, it can be seen that the coating adhesion increases with increasing gas pressure, while the coating adhesion also increases with increasing gas temperature, only not as significantly as with increasing gas pressure. The highest average value of adhesion at the coating/substrate interface is 69.8 N for the deposited coating at 900 °C and 5.5 MPa, and the lowest average value of adhesion at the coating/substrate interface is 35.6 N for the deposited coating at 600 °C and 4 MPa. The investigation of typical SEM pictures of scratches after testing (Figs. 6b-6e) shows that the length of the destruction area of the deposited coatings by the indenter (light area) in cold sprayed coatings. The critical load with the SEM images of the critical length of the scratch L_c after scratch testing for the coatings formed at 800 °C and different gas pressures is also given in Figs. 6b-6e. Compared with Figs. 6b-6e, the L_c increases with the increase of gas pressure, and the corresponding critical load also increases with increasing gas pressure. The delaminated position of the coatings from the substrate is exposed along the scratch direction when the applied load reaches the critical load. In Figs. 6b-6e, the highlighted morphologies of the scratch grooves are the delaminated coating positions, which are observed under the magnification as illustrated in the top left corner, respectively.

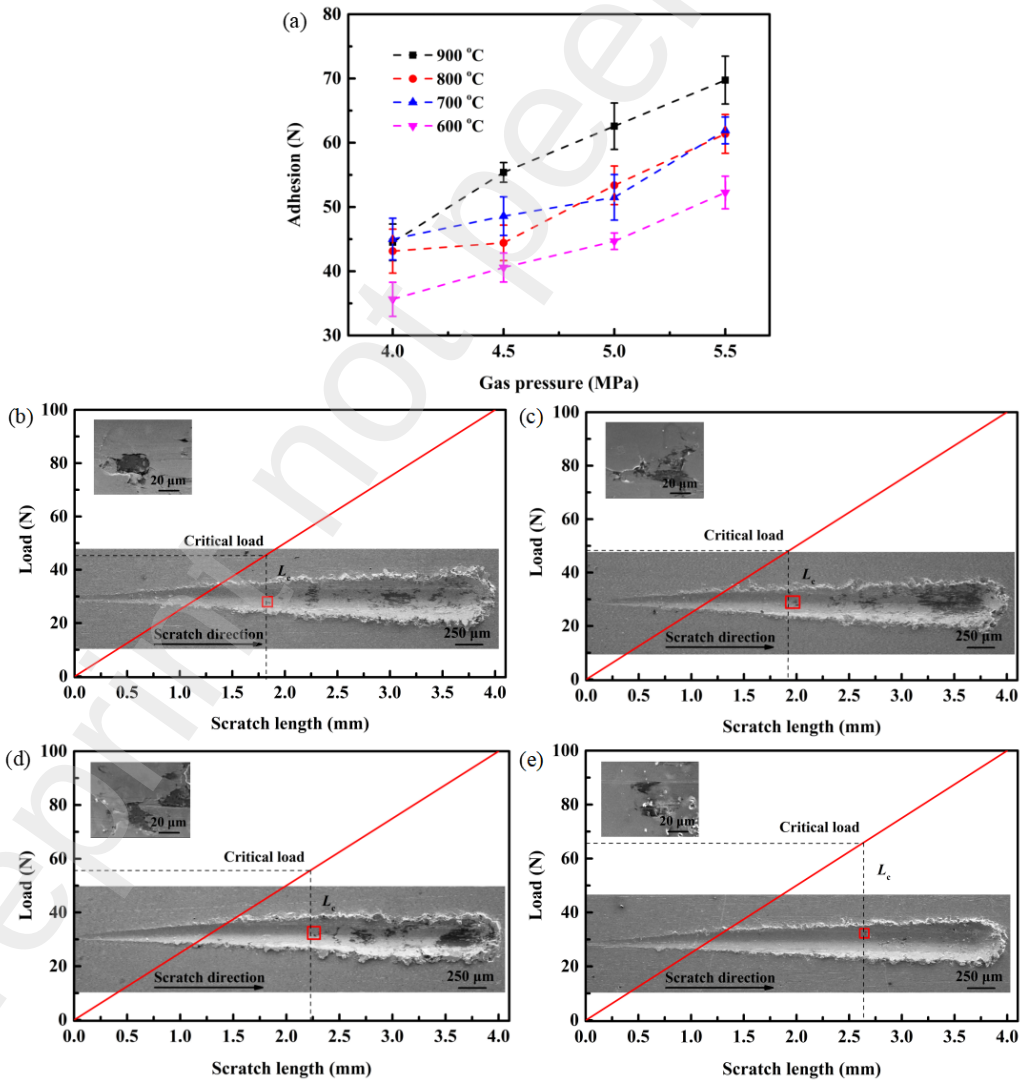

Fig. 6. Adhesion of Cu@Gr/CBC coatings on AA6061T6 substrate under different cold spray

parameters (a), and critical load with the SEM image of the critical length of the scratch L_c after scratch testing for the coatings formed at 800 ºC and different gas pressures: 4 MPa (b), 4.5 MPa (c),5 MPa (d) and 5.5 MPa (e). Magnification of the area noted by rectangular box in (b), (c), (d) and (e).

Particle velocity V_p is the most significant factor to determine the bonding strength and the effectiveness of jet formation of the deposited coatings [36]. The V_p can be given by the following equation,

$$V_p = \frac{V_g}{1+0.85\sqrt{\frac{D}{x}}\sqrt{\frac{\rho_p V_g^2}{p_o}}} \tag{2}$$

$$V_g = M\sqrt{\frac{\gamma RT}{M_w}} \tag{3}$$

Where V_g is gas velocity, D particle diameter, x axial position, ρ_p particle density, p_o supply pressure measured at the entrance of the nozzle, M local mach number=1.35, γ ratio of specific heats=1.4, T gas temperature, M_W molecular weight of the gas. Figure 7 shows the V_p under different cold spray parameters. As seen from Fig. 7, V_p increases by increasing the working temperature and pressure of the cold spray process gas. Because the V_g is higher, leading to larger accelerating drag, higher gas temperature increases V_p [37]. The surface roughness, thickness and adhesion of the single lane and single layer Cu@Gr/CBC coatings are all linear with V_p, as shown in Fig. 8. The surface roughness is a linear decrease relation with V_p, while the thickness and adhesion are a linear increase relation with V_p.

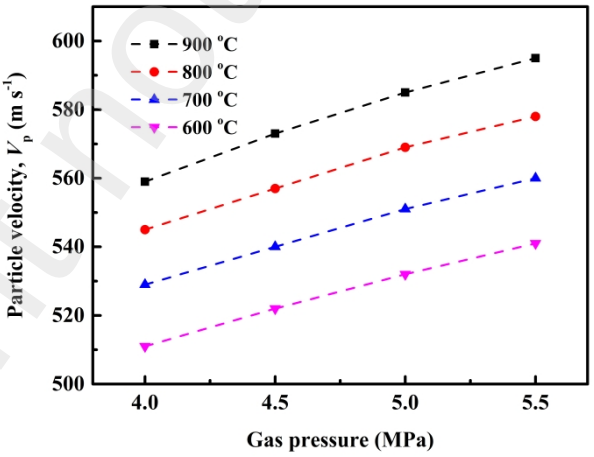

Fig. 7. Correlation of particle velocity V_p with gas temperatures and gas pressures for the cold sprayed coatings of the single lane and single layer Cu@Gr/CBC.

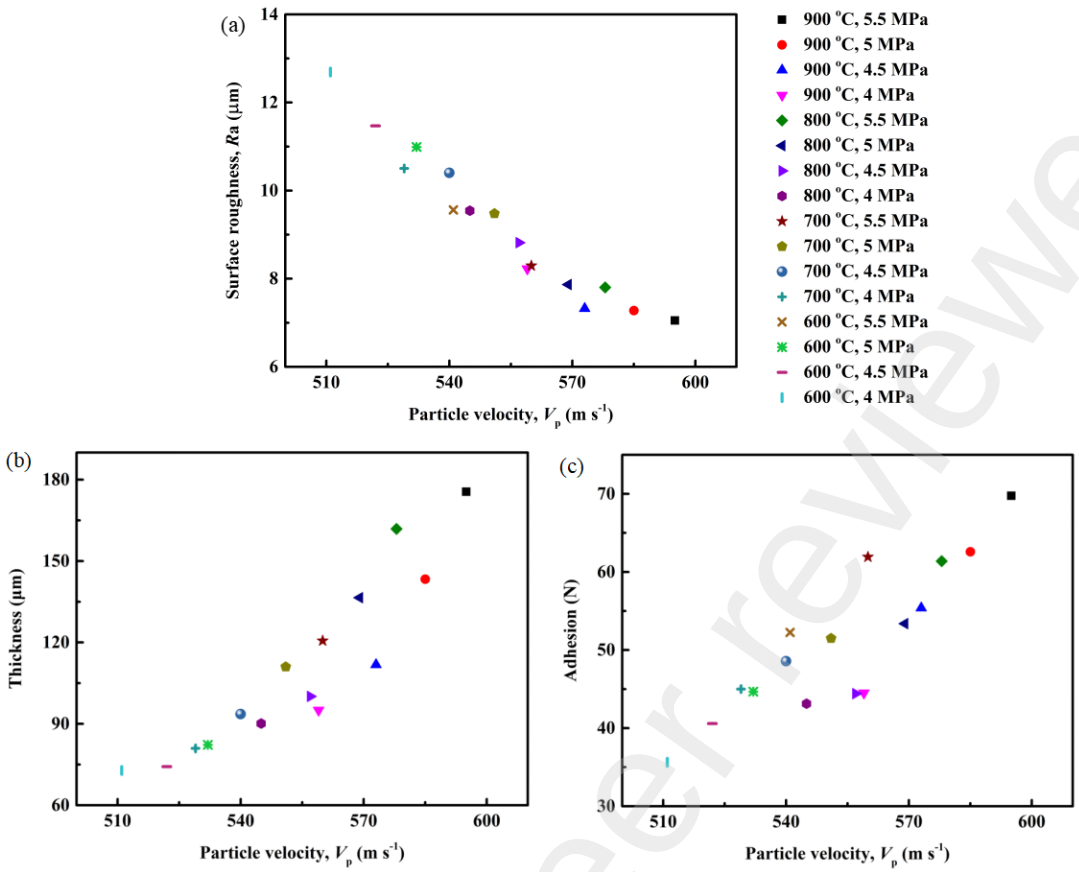

Fig. 8. Scaling of surface roughness, thickness, adhesion and particle velocity V_p for the cold sprayed coatings of the single lane and single layer Cu@Gr/CBC at different gas temperatures and gas pressures. Surface roughness as a function of V_p (a), correlation of thickness with V_p (b), and correlation of adhesion with V_p (c).

4. Conclusion

Cold sprayed coatings of the single lane and single layer Cu@Gr/CBC under different cold spray parameters have been successfully deposited on AA6061 T6 substrate by using N_2 as propellant gas. The *Ra* of the cold sprayed coatings is gradually decreased with increasing gas pressure and gas temperature. The thickness of the deposited coatings increases significantly with the increase of gas pressure and gas temperature. The critical load in the scratch test is used as a measure of scratch adhesion. The coating adhesion increases with the increase of gas pressure, while the coating adhesion also increases with increasing gas temperature, only not as significantly as with increasing gas pressure. When the coating is not oxidized, the Cu-coated graphite reinforced Cu based composite coating at 800 °C, 5.5 MPa possesses the lowest surface roughness, the maximum thickness and the highest adhesion among the cold sprayed coatings. The surface roughness of the single lane and single layer Cu@Gr/CBC coatings is a linear decrease relation with V_p, while the thickness and adhesion are a linear increase relation with V_p.

Acknowledgements

The authors would like to acknowledge the National Natural Science Foundation of China (No. 52201187), the Zhejiang Province key research and development plan project (2023C01082), the General Scientific Research Project of Zhejiang Provincial Education Department (No.

Y202249336), the Zhejiang Public Welfare Technology Application Research Project (No. LGC20E010003), the Science and Technology Plan Project of Taizhou (Nos. 22gya18, 21gya23, 2002gy06).

References

[1] M.S.A. Parast, M. Azadi. A short evaluation of simultaneous corrosion fretting fatigue behaviors in piston aluminium-silicon alloys considering effects of nano-particles and heat-treating, International Journal of Fatigue 168 (2023) 107403.
[2] F.G. Franceschini, O.R. Klegues Montedo, S. Arcaro, C.P. Bergmann. Aluminum borophosphate glaze-coated aluminum alloy substrate: Coating properties and coating/substrate coupling, Ceramics International 47 (2021) 2050-2057.
[3] Y. Huang, Y. Zhu, H. Li, S. Ma. Study on properties of alkaline copper coating by electro-brush plating on aluminium alloys surface, Hot Working Technology 35 (2006) 22-24.
[4] X. Wang, Y. Su, Q. Ouyang, C. Zhu, H. Cao, D. Zhang. Fabrication, mechanical and thermal properties of copper coated graphite films reinforced copper matrix laminated composites via ultrasonic-assisted electroless plating and vacuum hot-pressing sintering, Materials Science and Engineering: A 824 (2021) 141768.
[5] R. Zhao, W. Li, T. Wang, K. Zhan, Z. Yang, Y. Yan, B. Zhao, J. Yang. Fabrication of Cu/graphite film/Cu sandwich composites with ultrahigh thermal conductivity for thermal management applications, Frontiers of Materials Science 14 (2020) 188-197.
[6] S.-k. Jia, Y. Zou, J.-y. Xu, J. Wang, L. Yu. Effect of TiO_2 content on properties of Al_2O_3 thermal barrier coatings by plasma spraying, Transactions of Nonferrous Metals Society of China 25 (2015) 175-183.
[7] B. Sahoo, T. Das, J. Paul. Thermal spraying and related technologies for the surface modification of Al alloys: Review, Surface Review and Letters 29 (2022) 2230009.
[8] A. Ladwig, S. Babayan, M. Smith, M. Hester, W. Highland, R. Koch, R. Hicks. Atmospheric plasma deposition of glass coatings on aluminum, Surface and Coatings Technology 201 (2007) 6460-6464.
[9] S.P. Sahoo, S. Datta. Dry machining performance of AA7075-T6 alloy using uncoated carbide and MT-CVD TiCN-Al2O3-coated carbide inserts, Arabian Journal for Science and Engineering 45 (2020) 9777-9791.
[10] J.H. Ouyang, S. Nowotny, A. Richter, E. Beyer. Laser cladding of yttria partially stabilized ZrO_2 (YPSZ) ceramic coatings on aluminum alloys, Ceramics International 27 (2001) 15-24.
[11] Q. Wang, Q. Li, F. Chen, L. Zhang, J. Li, J. Zhang. Corrosion behavior of laser-cladding NiCrBSi coating in molten aluminum alloy, Journal of Laser Applications 34 (2022) 022022.
[12] F. Davoodi, F. Ashrafizadeh, M. Atapour, R. Rikhtehgaran. A novel approach for evaluation of load bearing capacity of duplex coatings on aluminum alloy using PLS and SVR models, Trans. Nonferrous Met. Soc. China 32 (2022) 1834-1851.
[13] N. Liu, J. Gao, S. Tong, L. Xu, Y. Wan, H. Sun. Improvement in corrosion resistance of micro‐arc oxidation coating on PVD, International Journal of Applied Ceramic Technology 19 (2022) 2556-2565.
[14] G. Lv, W. Gu, H. Chen, W. Feng, M.L. Khosa, L. Li, E. Niu, G. Zhang, S.-Z. Yang. Characteristic of ceramic coatings on aluminum by plasma electrolytic oxidation in silicate and phosphate electrolyte, Applied Surface Science 253 (2006) 2947-2952.
[15] S. Tong, L. Xu, Y. Wan, Y. Wang, J. Wang. Enhanced corrosion‐resistant performance of the

PEO coatings on AA7075 alloy by a sol-gel-derived silica layer, Int J Applied Ceramic Tech (2022).
[16] K. Chanyathunyaroj, W. Samit, C. Poonthananiwatkul, S. Phetchcrai. Effect of coatings on the mechanical properties and fatigue life of 6061 aluminum alloys, Transactions of the Indian Institute of Metals 74 (2021) 2135-2147.
[17] L. Winter, T. Lampke. Influence of hydrothermal sealing on the high cycle fatigue behavior of the anodized 6082 aluminum alloy, Coatings 12 (2022) 1070.
[18] T.A. Minto, V.M.C.A. de Oliveira, H.J.C. Voorwald. Plasma immersion ion implantation: Influence on the rotating bending fatigue strength of AA 7050-T7451 aluminum alloy, International Journal of Fatigue 103 (2017) 17-27.
[19] X. Zhao, T. Dong, B. Fu, G. Li, Q. Liu, Y. Li. Microstructure and properties of cold sprayed NiCrAl coating on AZ91D magnesium alloy, Coatings 11 (2021) 193.
[20] P. Cavaliere, A. Perrone, A. Silvello, A. Laska, G. Blasi, I.G. Cano, B. Sadeghi, S. Nagy. Cyclic behavior of FeCoCrNiMn high entropy alloy coatings produced through cold spray, Journal of Alloys and Compounds 931 (2023) 167550.
[21] Y. Wang, B. Normand, N. Mary, M. Yu, H. Liao. Effects of ceramic particle size on microstructure and the corrosion behavior of cold sprayed SiCp/Al 5056 composite coatings, Surface and Coatings Technology 315 (2017) 314-325.
[22] Z. Song, H. Li. Plasma spraying with wire feeding: A facile route to enhance the coating/substrate interfacial metallurgical bonding, Coatings 12 (2022) 615.
[23] P. Zhang, G. Zhang, J. Pan, C. Ma, G. Zhang. Non-isocyanate polyurethane coating with high hardness, superior flexibility, and strong substrate adhesion, ACS Appl Mater Interfaces 15 (2023) 5998-6004.
[24] M.B. Sedelnikova, K.V. Ivanov, A.V. Ugodchikova, A.D. Kashin, P.V. Uvarkin, Y. Sharkeev, T.V. Tolkacheva, A.I. Tolmachev, J. Schmidt, V.S. Egorkin, A.S. Gnedenkov. The effect of pulsed electron irradiation on the structure, phase composition, adhesion and corrosion properties of calcium phosphate coating on Mg0.8Ca alloy, Materials Chemistry and Physics 294 (2023) 126996.
[25] Z. Chen, K. Zhou, X. Lu, Y.C. Lam. A review on the mechanical methods for evaluating coating adhesion, Acta Mechanica 225 (2014) 431-452.
[26] M. Horgnies, P. Willieme, O. Gabet. Influence of the surface properties of concrete on the adhesion of coating: Characterization of the interface by peel test and FT-IR spectroscopy, Progress in Organic Coatings 72 (2011) 360-379.
[27] E.P. O'Brien, T.C. Ward, S. Guo, D.A. Dillard. Strain energy release rates of a pressure sensitive adhesive measured by the shaft-loaded blister test, The Journal of Adhesion 79 (2010) 69-97.
[28] H. Sharifi, M. Aliofkhazraei, G.B. Darband, S. Shrestha. A review on adhesion strength of peo coatings by scratch test method, Surface Review and Letters 25 (2018) 1830004.
[29] S. Nißen, J. Heeg, M. Wienecke, D. Behrend, M. Warkentin. Enhancing adhesion strength of a-C:H:Cu composite coatings on Ti6Al4V by graded copper deposition in a rf-PVD/PECVD hybrid process, Surface and Coatings Technology 350 (2018) 659-671.
[30] M.-Y. Cho, D.-W. Lee, P.-J. Ko, S.-M. Koo, J. Kim, Y.-K. Choi, J.-M. Oh. Adhesive Mechanism of Al2O3/Cu Composite Film via Aerosol Deposition Process for Application of Film Resistor, Electronic Materials Letters 15 (2019) 227-237.
[31] F.G. de Cerqueira Lima, U. Mescheder, G.L. Katona, H. Leiste, E. Özel, C. Müller, H. Reinecke. Influence of silicon doping type on the adhesion of seedless electrodeposited copper layers, Surface and Coatings Technology 349 (2018) 208-216.

[32] P. Breuninger, F. Krull, K. Huttenlochner, C. Müller-Reno, C. Ziegler, R. Merz, M. Kopnarski, S. Antonyuk. Microstructuring of steel surfaces via cold spraying with 316L particles for studying the particle-wall collision behavior, Surface and Coatings Technology 379 (2019) 125054.
[33] H. Sun, A. Billard, H. Luo, W.-T. Zheng, X.-L. Zheng, M.-J. Dai, S.-S. Lin, Q. Shi, F. Sanchette. Influence of carbon content on the mechanical properties of TiCN–Cu nanocomposite coatings prepared by multi-arc ion plating, Vacuum 187 (2021) 110139.
[34] M. Daroonparvar, H.R. Bakhsheshi-Rad, A. Saberi, M. Razzaghi, A.K. Kasar, S. Ramakrishna, P.L. Menezes, M. Misra, A.F. Ismail, S. Sharif, F. Berto. Surface modification of magnesium alloys using thermal and solid-state cold spray processes: Challenges and latest progresses, Journal of Magnesium and Alloys 10 (2022) 2025-2061.
[35] A.M. Ralls, M. Daroonparvar, A.K. Kasar, M. Misra, P.L. Menezes. Influence of friction stir processing on the friction, wear and corrosion mechanisms of solid-state additively manufactured 316L duplex stainless steel, Tribology International 178 (2023) 108033.
[36] F.J. Wei, B.Y. Chou, K.Z. Fung, S.Y. Tsai. Thermomechanical properties of cold-sprayed copper coatings from differently fabricated powders, Surface and Coatings Technology 434 (2022) 128128.
[37] J. Huang, W. Ma, Y. Xie, H. Fukanum, K. Zhang, G. Wang, R. Huang. Influence of cold gas spray processing conditions on the properties of 316L stainless steel coatings, Surface Engineering 35 (2019) 784-791.